



Deposited via The University of Leeds.

White Rose Research Online URL for this paper:

<https://eprints.whiterose.ac.uk/id/eprint/169101/>

Version: Accepted Version

---

**Article:**

Sadiq Al-Baghdadi, MAR, Noor, ZMH, Zeiny, A et al. (2020) CFD analysis of a nanofluid-based microchannel heat sink. *Thermal Science and Engineering Progress*, 20. 100685. ISSN: 2451-9049

<https://doi.org/10.1016/j.tsep.2020.100685>

---

© 2020, Elsevier. This manuscript version is made available under the CC-BY-NC-ND 4.0 license <http://creativecommons.org/licenses/by-nc-nd/4.0/>.

**Reuse**

This article is distributed under the terms of the Creative Commons Attribution-NonCommercial-NoDerivs (CC BY-NC-ND) licence. This licence only allows you to download this work and share it with others as long as you credit the authors, but you can't change the article in any way or use it commercially. More information and the full terms of the licence here: <https://creativecommons.org/licenses/>

**Takedown**

If you consider content in White Rose Research Online to be in breach of UK law, please notify us by emailing [eprints@whiterose.ac.uk](mailto:eprints@whiterose.ac.uk) including the URL of the record and the reason for the withdrawal request.

# CFD analysis of a nanofluid-based microchannel heat sink

Maher A.R. Sadiq Al-Baghdadi<sup>1</sup>, Zainab M.H. Noor<sup>2</sup>, Aimen Zeiny<sup>1,\*</sup>, Alan Burns<sup>3</sup>,  
Dongsheng Wen<sup>3</sup>

<sup>1</sup> Kufa Centre for Advanced Simulation in Engineering (KCASE), Department of Mechanical Engineering, Faculty of Engineering, University of Kufa, Najaf, Iraq.

<sup>2</sup> Faculty of Basic Education, University of Kufa, Najaf, Iraq.

<sup>3</sup> School of Chemical and Process Engineering, University of Leeds, Leeds, UK.

## Abstract

Effective thermal management is a key for the continuous development of electronics, which are characteristics of modern life. It has a great effect on the lifetime, durability and reliability of these systems. A liquid-cooled microchannel heat sink is a compacted cooling part that used to provide better heat dissipation rates and low temperatures in electronic components. Nanofluids have been introduced as effective coolants to be employed in this type of heat sinks to increase the heat dissipation rates. However, a comparative assessment of the thermal performance between commonly used nanofluids and water as coolants for microchannel heat sinks is still lacking. For this purpose, a computational fluid dynamics (CFD), non-isothermal, three-dimensional detailed model has been developed to simulate and analyze the fluid flow and heat transfer physiognomies. The results show that examining performance parameters as function of Reynolds number is misleading since the thermophysical properties are different

among each coolant, and employing nanofluids in a microchannel heat sink is impractical and using water is cheaper and safer.

**Keywords:** MEMS; Microchannel heat sink; CFD; Nanofluids; Electronics cooling; Heat transfer.

## 1. Introduction

The high-power density and the compactness of the modern electronic packages push towards finding efficient and compact cooling components for high heat generation chips. The main function of these components is to keep the electronic packages within the design operating temperature range. Unlike traditional heat sinks, which need a large surface area to upturn heat dissipation rates, microchannel heat sinks seem to be fit for this purpose because they are small in size and effective in performance.

A microchannel heat sink bases on using small diameter passages for a liquid-coolant. These small diameter passages ensure a large area for the heat transfer between the chip and the coolant, enhancing the heat transfer rate [1]. However, using microchannel heat sinks in cooling electronic packages inflicts stark limits on the packages' design. At a certain heat generation rate, the temperature rise, pressure drop, and flow rate of the coolant necessitate optimization of the microchannel heat sink to dissipate that heat effectively.

Many researchers studied numerically the performance of different microchannel heat sinks with different geometrical designs of the flow field channels [2]–[11]. Their results have shown that changes in the geometrical design of the flow field channels can lead to higher heat transfer coefficients, but unfortunately, with an increase in pressure drop and friction factor comparing with the traditional smooth microchannels. Therefore, nanofluids have been proposed to be employed in microchannel heat sinks as super-coolants to enhance heat removal due to their highly effective thermal conductivity [12], [13]. However, It is well-known that the heat transfer coefficient ( $h$ ), which is a description of the heat transfer

effectiveness, is directly proportional to the thermal conductivity ( $k$ ), density ( $\rho$ ) and specific heat capacity ( $c_p$ ) and inversely proportional to the viscosity ( $\mu$ ) and surface tension ( $\sigma$ ), if phase change is involved [14]. Although seeding nanoparticles in liquids may increase the effective thermal conductivity and density, it may increase the effective viscosity and decrease the effective specific heat capacity of the nanofluids [14]–[16]. Therefore, a comprehensive investigation is essential to figure out the advantages and disadvantages of using nanofluids in microchannel heat sinks.

Computational Fluid Dynamics (CFD) methods are powerful tools to simulate fluid flow and the related heat and mass transfer by numerically solving mathematical equations that govern these processes, utilizing the rapid and continuous developments in computers and computing techniques. The results of the CFD simulations are relevant in: comprehensive detailed analysis; conceptual studies of re-design and new designs; in-depth product research and development; and troubleshooting [17]. CFD is very important in simulations of micro-electro-mechanical-systems (MEMS) applications, especially in the design of efficient microchannel heat sinks, because CFD can provide comprehensive information, visualized, and deeply detailed investigation comparing to analytical fluid dynamics and also experimental fluid dynamics. Using CFD simulation models in production and design reduces the time and cost compared to the experimental-based method, along with CFD can solve a wide range of complex problems where the analytical methods have not [18], [19]. Consequently, CFD improves the fundamental understanding of fluid flow, mass and heat transfer characteristics, which are crucial in design and process control of microchannel heat sinks.

Many studies [20]–[26] examined numerically and/or experimentally the effect of employing nanofluids on the performance of microchannel heat sinks. In those studies, the Reynolds number was assumed to be the independent variable and the others, such as the Nusselt's number, heat transfer coefficient, pressure drop, and friction factor, are dependents. However, since the thermophysical properties of nanofluids differ than those of water depending on the concentration of the suspended nanoparticles, analyzing the performance of a microchannel

basing only on the Reynolds number is misleading [24], [27]. Therefore, another factor must be taken in consideration. Pumping power is one of the most important factors that must be considered in cost effective designs, and we have noticed that there is a lack in studying the performance variables as functions of pumping power.

In this work, a full three-dimensional, non-isothermal CFD model has been developed to evaluate the practical benefit of using nanofluids as coolants in a microchannel heat sink in the thermal management of micro-electro-mechanical-systems (MEMS) devices. The detailed analysis of the heat transfer and fluid flow has been conducted for various types of nanofluids.

## **2. Microchannel heat sink computational model**

### *2.1. Computational domain*

The model presented in this study is a complete full three-dimensional, steady-state, single-phase, non-isothermal model. The microchannel heat sink consists of 50 straight channels with a rectangular cross-section. A computational model of an entire heat sink would need huge computing resources and unreasonably very long time for simulation. Due to the symmetry, the computational domain in this study is then limited to a symmetric unit only, which consists of one straight flow microchannel with its ribs, and has dimensions of a total height of (0.35 mm), a width of (0.2 mm), and a length of (10 mm). The flow field region has a height of (0.2 mm) and a width of (0.1 mm). The thickness of the microchannel bottom plate is (0.15 mm). The full computational domain is shown in Figure 1.

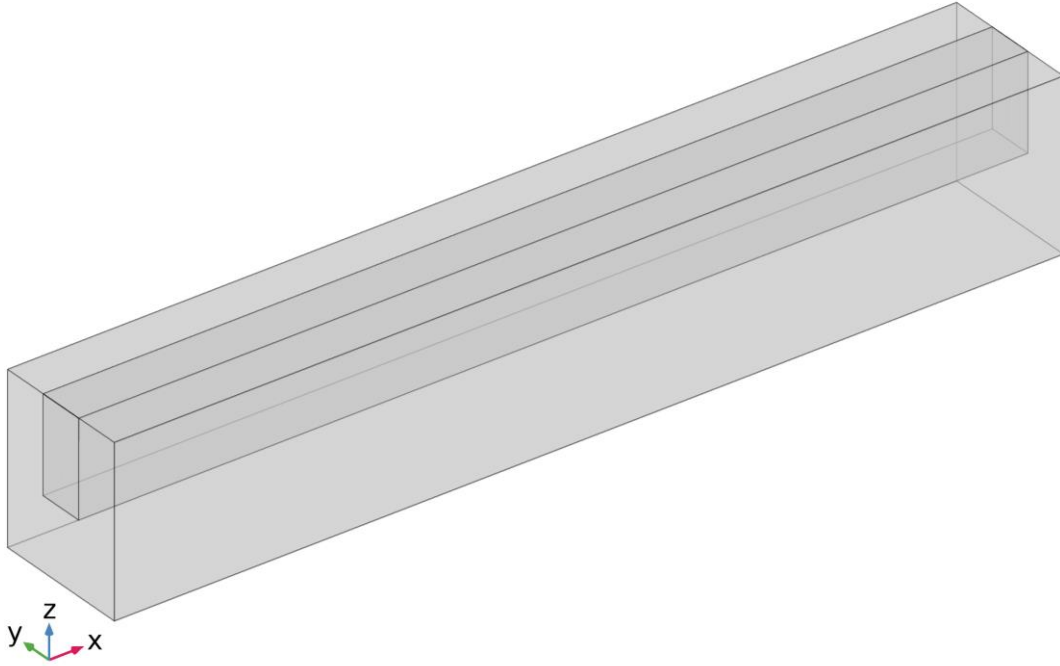


Figure 1. Three-dimensional computational domains.

## 2.2. Conservation equations

The coolant-flow field is incompressible, single-phase, laminar flow across a microchannel and it is obtained by solving the steady-state Navier-Stokes equations.

Mass conservation equation;

$$\nabla \cdot (\rho_f \cdot u) = 0 \quad (1)$$

Momentum equation

$$(u \cdot \nabla) \cdot \rho_f \cdot u = -\nabla p + \mu_f \cdot \nabla^2 u \quad (2)$$

where  $u$ ,  $\rho_f$ ,  $p$ , and  $\mu_f$  are the velocity [m/s], density [kg/m<sup>3</sup>], pressure [Pa], and dynamic viscosity [N.s/m<sup>2</sup>] of the coolant respectively.

Energy equation

$$u. \nabla T = \frac{k_f}{\rho_f.Cp} \nabla^2 T \quad (3)$$

where  $k_f$ , and  $Cp$  are the thermal conductivity [W/m.K] and specific heat [J/kg.K] of the coolant respectively.  $T$  is the temperature [K].

Energy equation for the solid region (silicon)

$$k_s. \nabla^2 T = 0 \quad (4)$$

where  $k_s$  is the thermal conductivity of the silicon [W/m.K]. Subscripts "f" and "s" refer to fluid (coolant) and solid (silicon), respectively.

### 2.3. Thermophysical properties of the coolant

The thermophysical properties of the base fluid "bf" (i.e. water) depend on temperature and can be obtained using the following equations [22], [28];

$$\rho_{bf} = \frac{999.84 + 18.225(T+273.15) - 7.92 \times 10^{-3}(T+273.15)^2 - 5.545 \times 10^{-5}(T+273.15)^3 + 1.498 \times 10^{-7}(T+273.15)^4 - 3.933 \times 10^{-10}(T+273.15)^5}{1 + 1.816 \times 10^{-2}(T+273.15)} \quad (5)$$

$$\mu_{bf} = 2.414 \times 10^{-5} \times 10^{\frac{247.8}{T-140}} \quad (6)$$

$$Cp_{bf} = 8958.9 - 40.535T + 0.11243T^2 - 1.014 \times 10^{-4}T^3 \quad (7)$$

$$k_{bf} = -0.58166 + 6.3556 \times 10^{-3}T - 7.964 \times 10^{-6}T^2 \quad (8)$$

The thermophysical properties of the nanofluids "nf" depend on the volume fraction  $\phi$  of the nanoparticles "np" in the suspension and can be obtained using the following equations[22];

$$\rho_{nf} = (1 - \phi) \cdot \rho_{bf} + \phi \rho_{np} \quad (9)$$

$$\rho_{nf} C_{p_{nf}} = (1 - \phi) \cdot \rho_{bf} C_{p_{bf}} + \phi \rho_{np} C_{p_{np}} \quad (10)$$

The empirical correlation of the thermal conductivity based on the Brownian motion of nanoparticles are given as

$$k_{eff} = k_{static} + k_{Brownian} \quad (11)$$

The static thermal conductivity is given as

$$k_{static} = k_{bf} \left[ \frac{k_{np} + 2k_{bf} - 2(k_{bf} - k_{np})\phi}{k_{np} + 2k_{bf} + (k_{bf} - k_{np})\phi} \right] \quad (12)$$

Brownian thermal conductivity is given as

$$k_{Brownian} = 5 \times 10^4 \beta \cdot \phi \cdot \rho_{bf} \cdot C_{p_{bf}} \sqrt{\frac{\sigma_B \cdot T}{\rho_{np} \cdot d_{np}}} \cdot f(T, \phi) \quad (13)$$

$$f(T, \phi) = (2.8217 \times 10^{-2} \cdot \phi + 3.917 \times 10^{-3}) \left( \frac{T}{T_0} \right) + (-3.0699 \times 10^{-2} \cdot \phi - 3.91123 \times 10^{-3}) \quad (14)$$

where  $\sigma_B$  is the Boltzmann constant, and  $\beta$  is the fraction of the liquid volume moving with the nanoparticles (Table 1).

Table 1. Values of  $\beta$  for different types of nanoparticles

Nanoparticles	$\beta$	Volume fraction [%]	Temperature [K]
SiO <sub>2</sub>	$1.9526(100\phi)^{-1.45940}$	1 % $\leq \phi \leq$ 10 %	298 $\leq T \leq$ 363 K

Al <sub>2</sub> O <sub>3</sub>	8.4407(100 $\phi$ ) <sup>-1.07304</sup>	1 % ≤ $\phi$ ≤ 10 %	298 ≤ T ≤ 363 K
CuO	9.8810(100 $\phi$ ) <sup>-0.94460</sup>	1 % ≤ $\phi$ ≤ 06 %	298 ≤ T ≤ 363 K

The empirical correlation of the dynamic viscosity is given as

$$\mu_{eff} = \mu_{static} + \mu_{Brownian} \quad (15)$$

$$\mu_{static} = \frac{\mu_{bf}}{(1-\phi)^{2.5}} \quad (16)$$

$$\mu_{Brownian} = 5 \times 10^4 \beta \cdot \phi \cdot \rho_{bf} \cdot \sqrt{\frac{\sigma_B \cdot T}{\rho_{np} \cdot d_{np}}} \cdot f(T, \phi) \quad (17)$$

where  $d_{np}$  is the diameter of nanofluids particles [nm],  $M$  is the molecular weight of the base fluid,  $G$  is the Avogadro number.

The thermophysical properties of the base fluid (water) and nanoparticles (SiO<sub>2</sub>, Al<sub>2</sub>O<sub>3</sub>, CuO) evaluated at 300 K are presented in Table 2. The effective thermophysical properties of each nanofluid at  $\phi = 4\%$  and  $d_{np} = 30$  nm are summarized in Table 3.

Table 2. The thermophysical properties of base fluid (water) and different types of nanoparticles at T=290K [22].

Thermophysical properties	Water	SiO <sub>2</sub>	Al <sub>2</sub> O <sub>3</sub>	CuO
Density $\rho$ [kg/m <sup>3</sup> ]	998.2	2200	3970	6500
Dynamic viscosity $\mu$ [Pa.s]	0.001	0	0	0
Thermal conductivity $k$ [W/m.K]	0.60	1.2	40	20
Specific heat $C_p$ [J/kg.K]	4182	495.2	765	535.6

Table 3. The effective thermophysical properties of each nanofluid at  $\phi = 4\%$  and  $d_{np} = (30 \text{ nm})$ .

	Water + SiO <sub>2</sub>	Water + Al <sub>2</sub> O <sub>3</sub>	Water + CuO
Density $\rho_{eff}$ [kg/m <sup>3</sup> ]	1046.30	1117.1	1182.3
Dynamic viscosity $\mu_{eff}$ [Pa.s]	0.00110721	0.00110613	0.00110589
Thermal conductivity $k_{eff}$ [W/m.K]	0.61718	0.66611	0.66193
Specific heat $Cp_{eff}$ [J/kg.K]	3871.91	3696.25	3491.13

#### 2.4. Thermophysical properties of the microchannel heat sink

Silicon is used as the microchannel heat sink in this work. The thermophysical properties of silicon are listed in Table 4.

Table 4. The thermophysical properties of heat sink material.

Material	Density $\rho_s$ [kg/m <sup>3</sup> ]	Thermal conductivity $k_s$ [W/m.K]	Specific heat $Cp_s$ [J/kg.K]	Young's modulus $E_s$ [Pa]	thermal expansion $\beta$ [1/K]	Poisson's ratio $\alpha$
Silicon	2329	130	700	170e <sup>9</sup>	2.6e <sup>-6</sup>	0.28

#### 2.5. Computational procedure and boundary conditions

The finite-volume method was used to discretize the governing equations, which are in turn solved using a commercial CFD code having the power to address multi-physics problems. A computational quadratic mesh has been used in this model. Severe numerical trials were executed to confirm that the solutions of the model were independent of the grid size. Grid sensitivity has been performed to ensure that the solutions acquired using the selected mesh is

independent of the grid size. The selected grid consists of 563140 domain elements in total, 46832 boundary elements, and 2661 edge elements, which was found to provide enough resolution (Figure 2). An iterative solution for the coupled equations was followed, where an error criterion of  $1.0 \times 10^{-6}$  was considered sufficient enough to achieve the solution convergence. The solution of the calculated variables in the model was measured to be convergent when the comparative error was less than in each field between two consecutive iterations.

Boundary and initial conditions are specified for the present model as follows. A uniform axial velocity and uniform temperature are used as the inlet velocity and temperature conditions, respectively. The pressure outlet is subjected to the outlet side. The bottom wall of the microchannel is fixed and subjected to uniform heat flux ( $1 \times 10^6 \text{ W/m}^2$ ). Wide ranges of the Reynolds numbers are used in the range from 100 to 1000 on the thermal and flow fields.

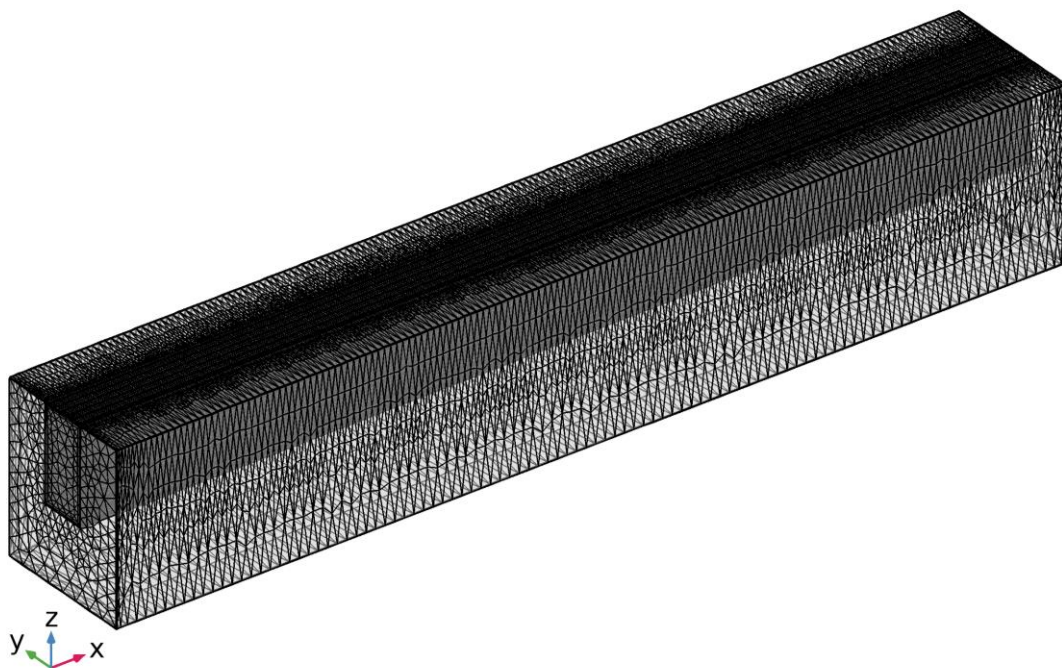


Figure 2. Three-dimensional computational quadratic mesh of the domain.

## 2.6. Data acquisition

The performance factors and the analytical parameters that characterize each of the fluid flow of the coolant and the heat transfer inside the microchannel heat sink are defined as

The Reynolds number is given as

$$Re = \frac{\rho_f u_m D_h}{\mu_f} \quad (18)$$

where  $u_m$  is the average velocity of the coolant flow at the inlet of the microchannel [m/s],  $D_h$  is the hydraulic diameter of the microchannel [m].

The hydraulic diameter of the microchannel is calculated as

$$D_h = \frac{2WH}{W+H} \quad (19)$$

where  $W$  and  $H$  are the width and height of the microchannel respectively [m].

The average friction factor denoting the resistance force is defined as

$$\bar{f} = \frac{\Delta p D_h}{2\rho_f L u_m^2} \quad (20)$$

where  $\Delta p$  is the coolant pressure drop [Pa] through the microchannel length ( $L$ ) [m].

The average heat transfer coefficient is given as

$$\bar{h} = \frac{q A_q}{A_c (\bar{T}_c - \bar{T}_f)} \quad (21)$$

where  $q$  is the heat flux that applied to the bottom wall of the micro heat sink [W/m<sup>2</sup>],  $A_q$  is the heated area (i.e. silicon base area) [m<sup>2</sup>],  $A_c$  is the conjugated area (i.e. the area of the solid-fluid interface) [m<sup>2</sup>],  $\bar{T}_c$  is the conjugated area average temperature [K],  $\bar{T}_f$  is the mass-average temperature of coolant in the microchannel [K].

$$\bar{T}_c = \frac{\int T dA}{\int dA} \quad (22)$$

$$\bar{T}_f = \frac{\int T \rho_f dV}{\int \rho_f dV} \quad (23)$$

The average Nusselt number is given as

$$\overline{Nu} = \frac{\bar{h} D_h}{k_f} \quad (24)$$

The overall thermal resistance is well-defined as

$$R_T = \frac{T_{wall,max} - T_{f,in}}{q} \quad (25)$$

The pumping power of the microchannel heat sink for a steady flow of coolant is defined as

$$P = N \cdot u_m \cdot \Delta p \cdot A_{cs} \quad (26)$$

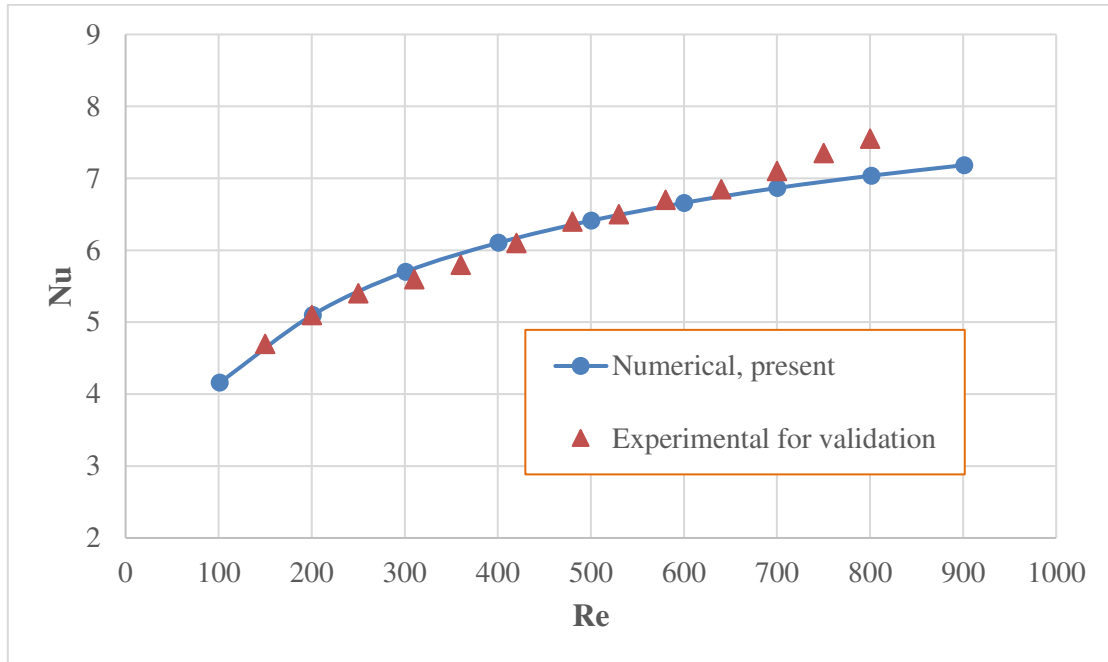
where N is the total number of the microchannels and  $A_{cs}$  is the cross-sectional area of the flow of each microchannel [m<sup>2</sup>].

### 2.7. Model validation

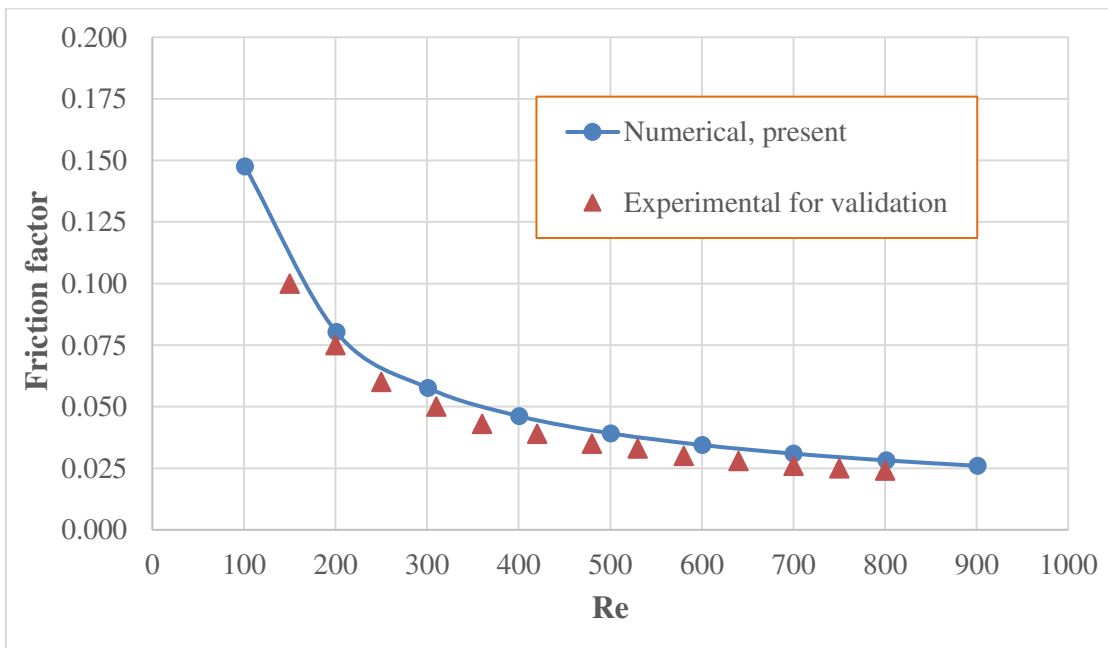
Validations of Nusselt number and the friction factor of the microchannel heat sink working with base fluid (water) are performed by comparing the results of the present numerical model with the experimental results obtained by Chai et al. [29] as presented in Figure 3. The modeling results approve well with the experimental results, which indicate the reliability of the model used in the present work.

Having completed the validation of the numerical simulation program by comparison with offered experimental data from the scientific literature, the following section present the CFD

results of the heat transfer, coolant flow structure, in addition to the pressure drop through the microchannel of the heat sink working by different types of nanofluids.



(a)



(b)

Figure 3. Model validation by comparing the present numerical results of the microchannel heat sink for water base fluid with Chai et al. experiments [29]. (a) Average Nusselt number, (b) average Friction factor.

### **3. Results and discussion**

#### *3.1. Velocity distribution*

Figures 4-6 show comparisons of the velocity distribution of the flow fields of different coolants (i.e., water, water-SiO<sub>2</sub>, water-Al<sub>2</sub>O<sub>3</sub>, and water-CuO) at different Reynolds numbers (i.e., 100, 500, and 900). Each figure shows differences among the velocity distributions of the four coolants although the Re is constant. This is due to the differences in the physical properties of each coolant (i.e., density and dynamic viscosity). The case of the water-CuO has the lowest velocity comparing with the other coolants. The cases of water and water-Al<sub>2</sub>O<sub>3</sub> have almost identical velocity distributions. While the case of water-SiO<sub>2</sub> has the highest velocity distribution. This is understandable as the inlet velocities are in the order from the highest to lowest (depending on the coolants densities and viscosities) as follows: water-SiO<sub>2</sub>; water and water-Al<sub>2</sub>O<sub>3</sub>; water-CuO, as can be seen in Figure 7. It is obvious that as Re increases, the difference among the velocity distributions becomes more clear.

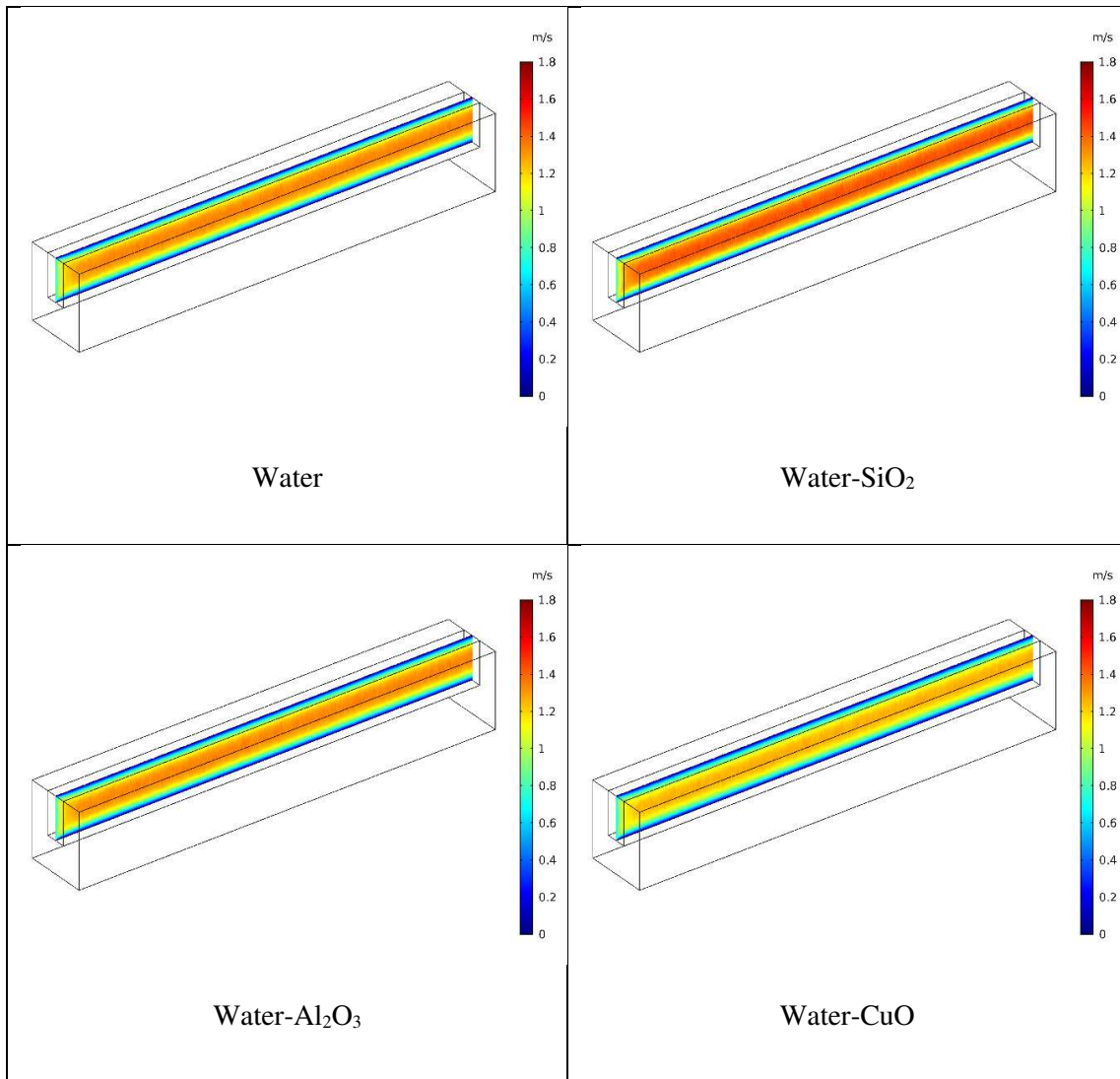
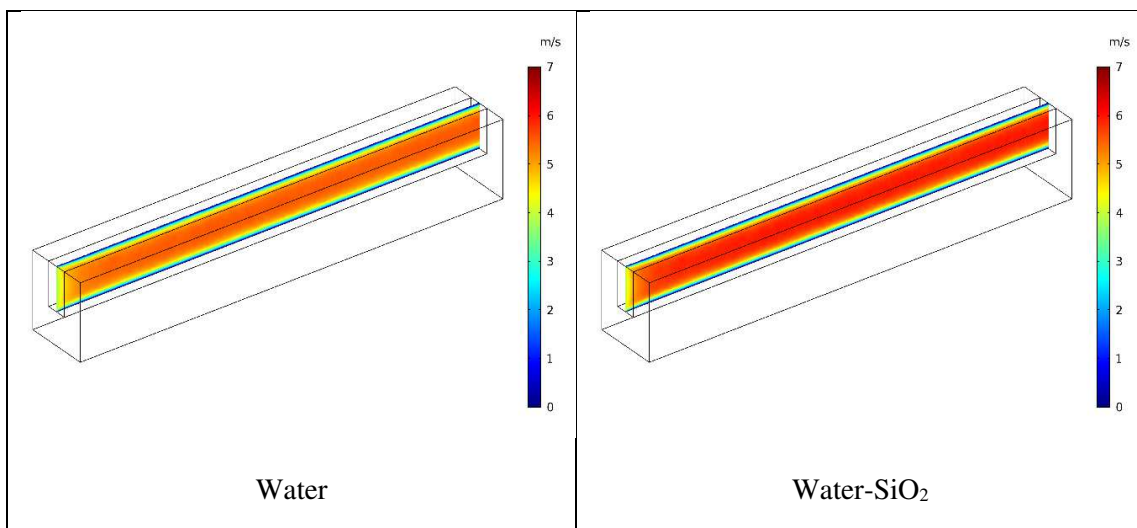


Figure 4. Coolant velocity distributions in the microchannel heat sink at 100 Reynolds number.



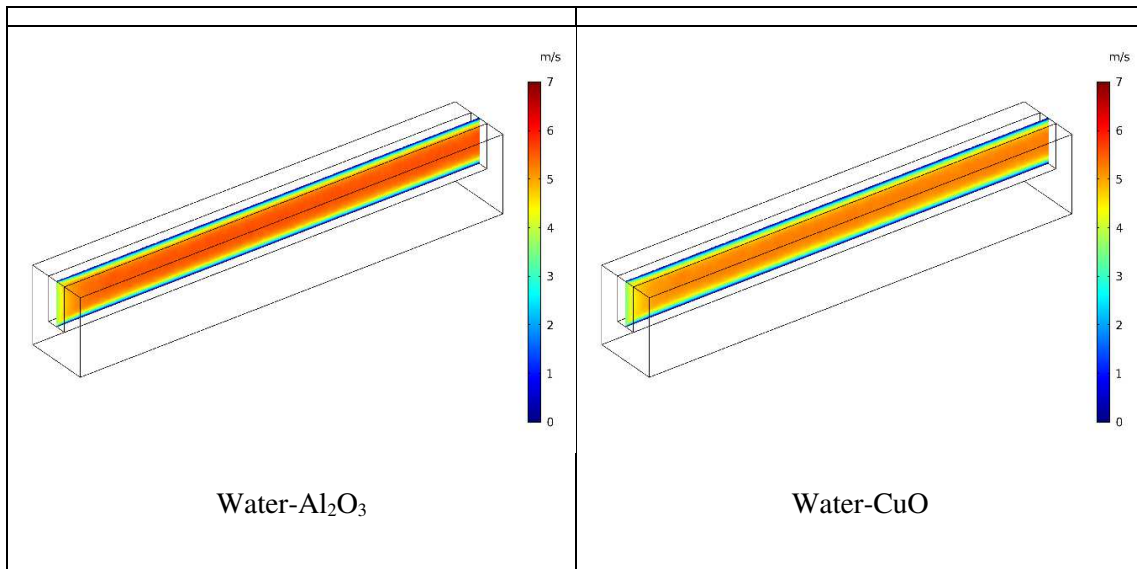


Figure 5. Coolant velocity distributions in the microchannel heat sink at 500 Reynolds number.

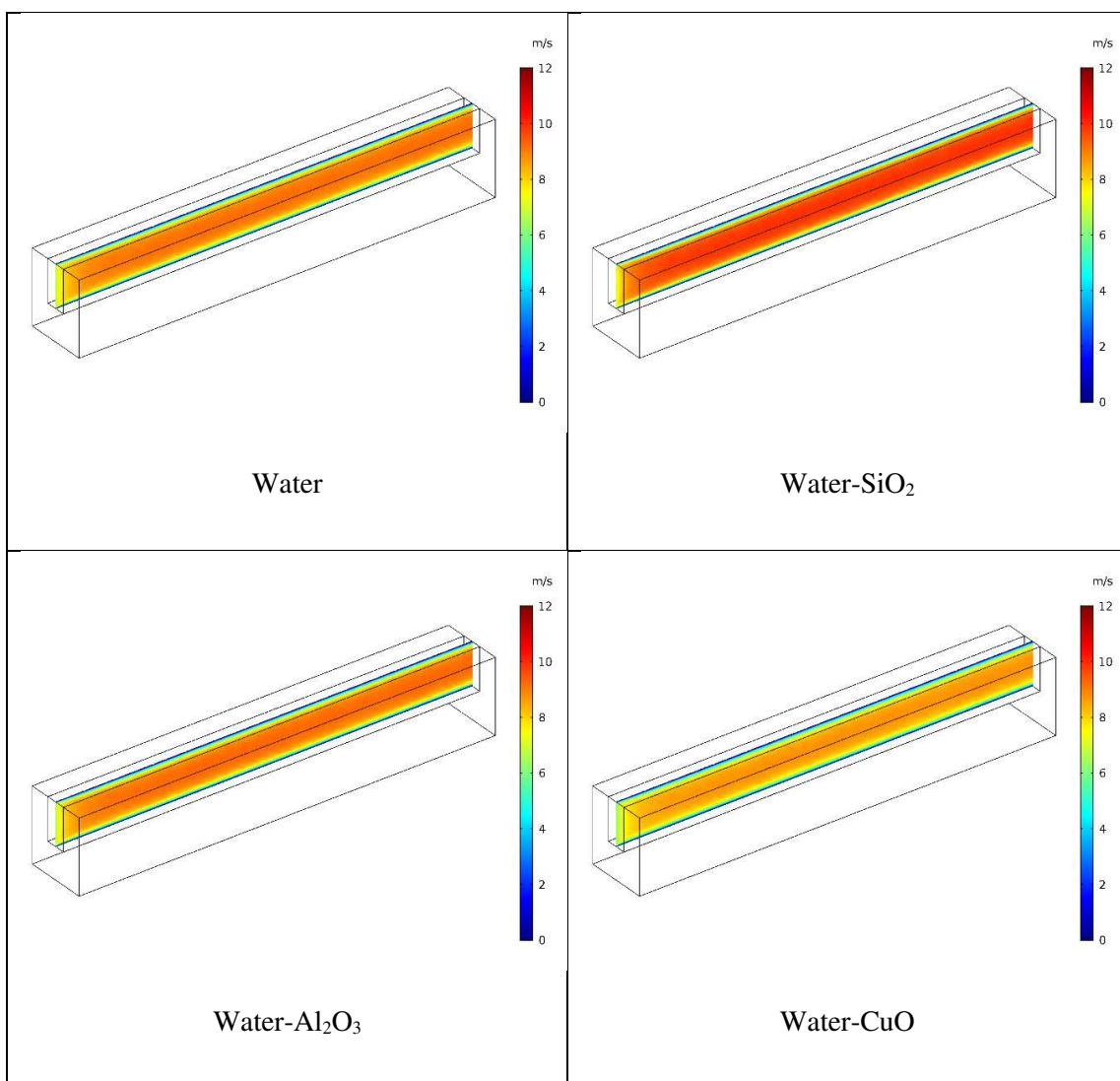


Figure 6. Coolant velocity distributions in the microchannel heat sink at 900 Reynolds number.

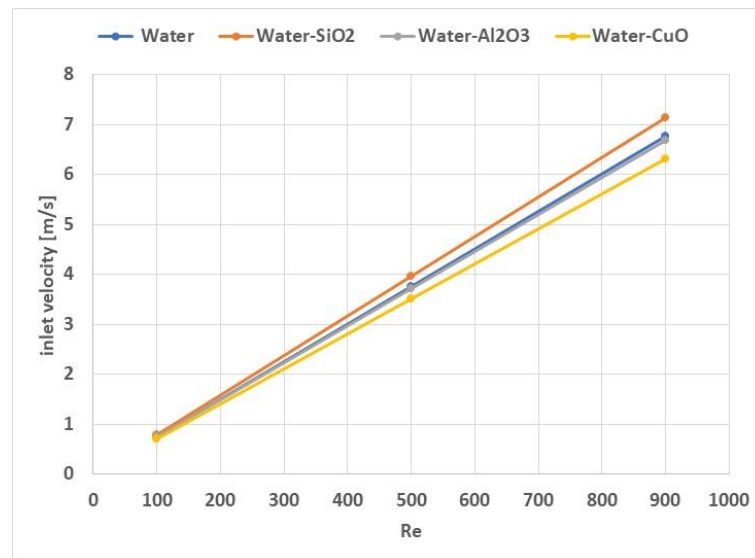


Figure 7. Inlet velocity of the coolants at different Re.

### 3.2. Pressure drop

The pressure distributions inside the microchannel working with different coolants at different Re are shown in Figures 7-9. The figures show that the pressure for all types of coolants decreases along the microchannel length of the heat sink. It is clear that the maximum pressure drop is in the case of water-SiO<sub>2</sub>. This is of course due to the higher velocity and dynamic viscosity of water-SiO<sub>2</sub>, as can be seen in Figures 7 and 10. The minimum pressure drop is clearly achieved in the case of water as coolant. These results suggest that using water-SiO<sub>2</sub> at a certain Re will need higher pumping power comparing with the other coolants. Although water has the lowest dynamic viscosity, it cannot be charged that using water needs the lowest pumping power as its inlet velocity is higher than that of water-CuO, as seen in Figure 7. Therefore, critical investigation is essential to decide which is the practical coolant that enhances the heat transfer rate and reduces the pumping power cost.

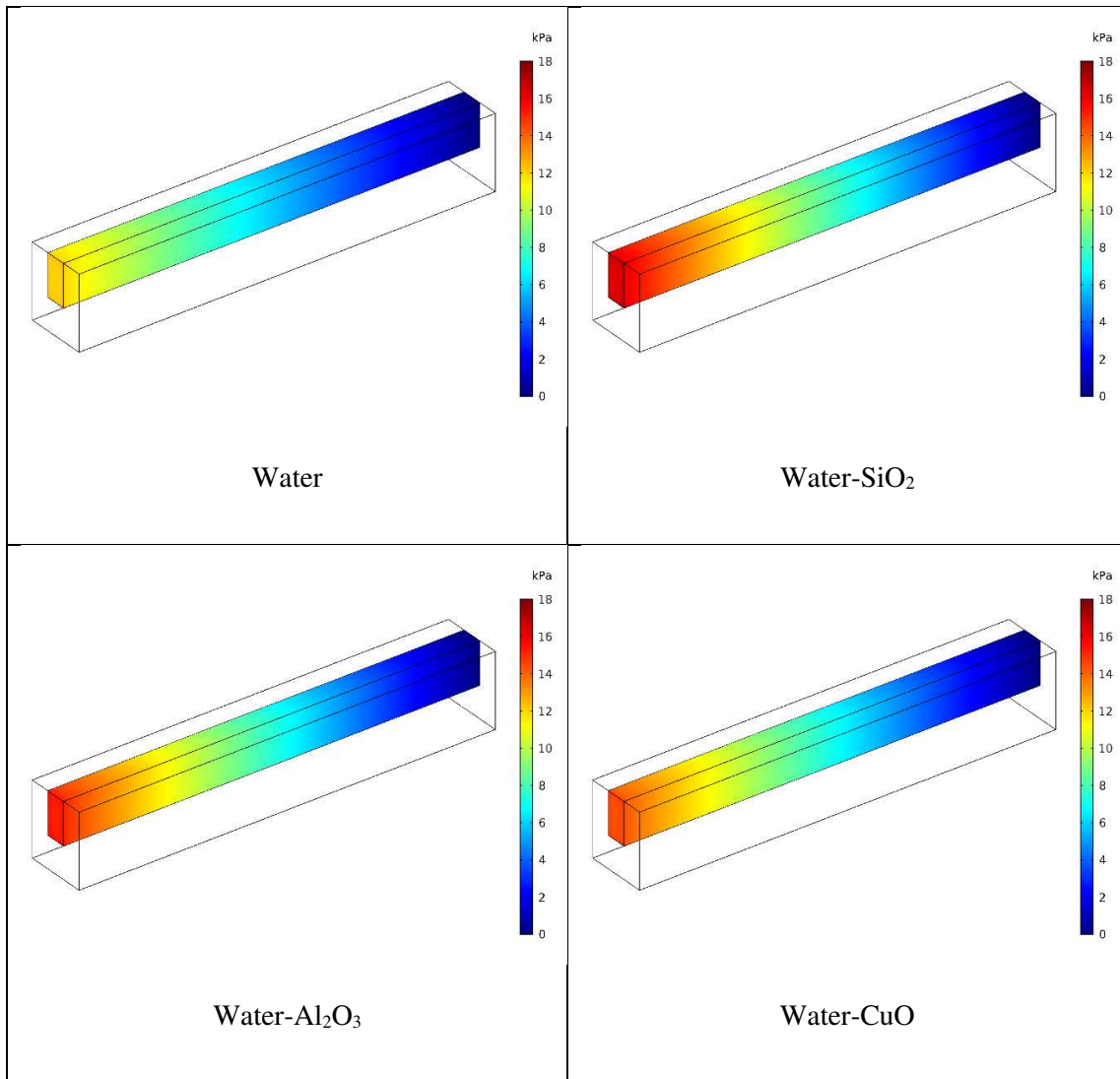
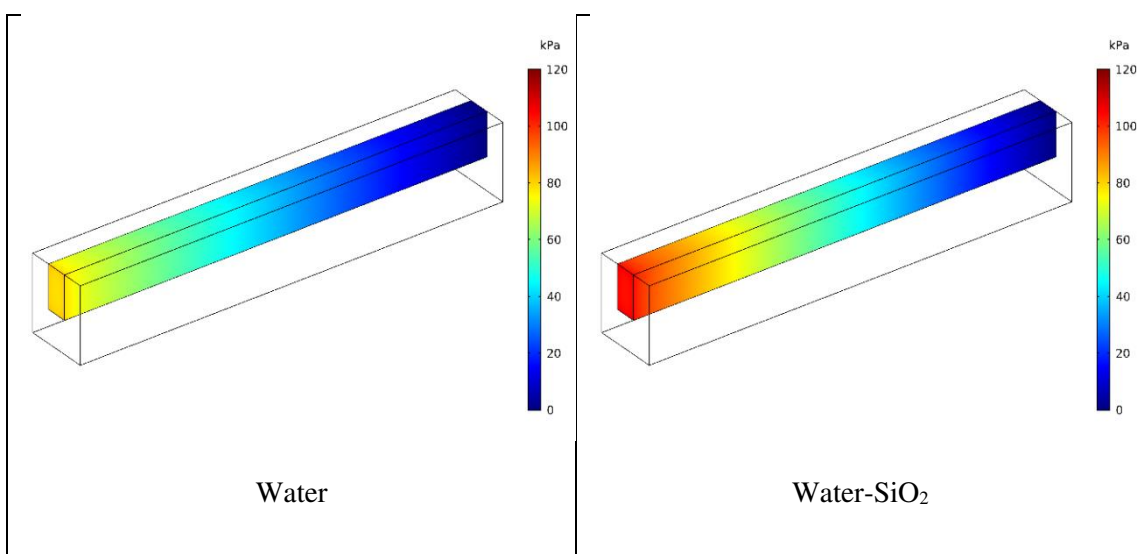


Figure 7. Coolant pressure distributions inside the microchannel heat sink at 100 Reynolds number.



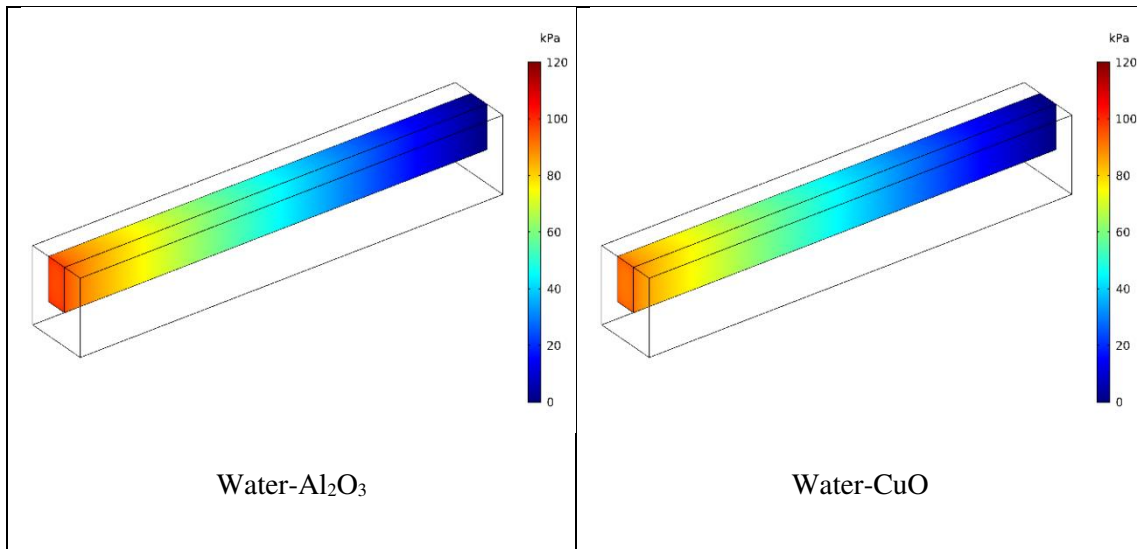


Figure 8. Coolant pressure distributions inside the microchannel heat sink at 500 Reynolds number.

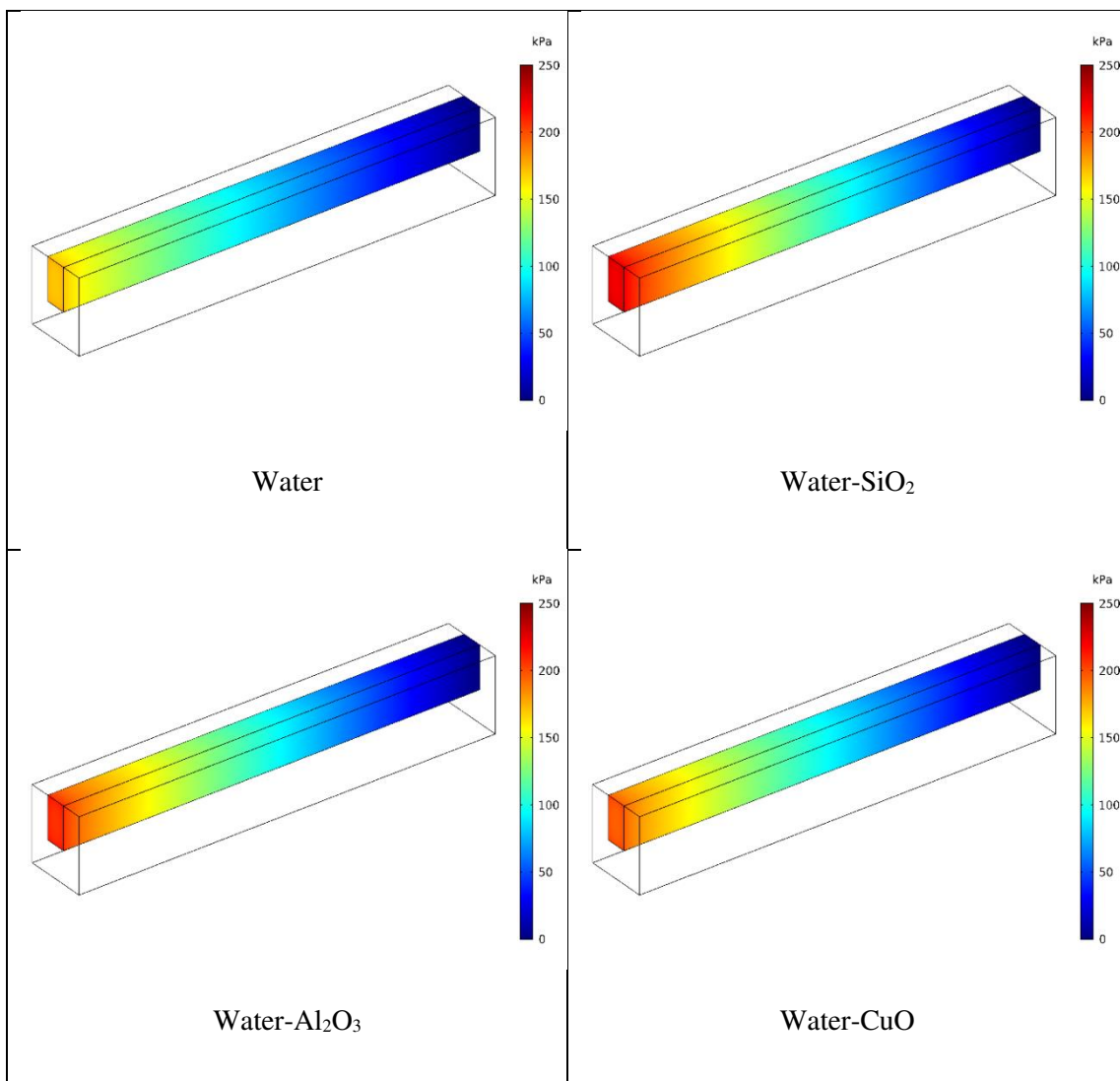


Figure 9. Coolant pressure distributions inside the microchannel heat sink at 900 Reynolds number.

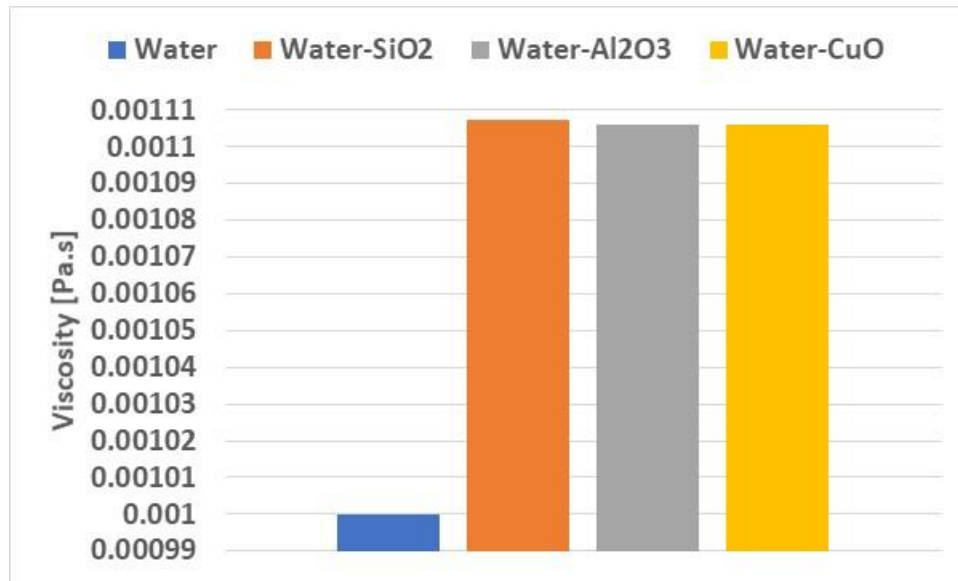


Figure 10. Dynamic viscosity of the different coolants.

### 3.3. Heat transfer

With the aim of analyzing the local heat transfer enhancement, Figures 11-13 show the temperature distributions in the microchannel heat sink for the different coolants with a range of the Reynolds numbers. The figures show that the maximum temperature occurs at the heated bottom wall of the heat sink where the electronic semiconductor chips are attached. In addition, for the coolant flow, the temperature values rise through the flow direction, and the maximum value of the temperature takes place at the exit of the microchannel. At this stage it is really difficult to decide which coolant enhances the heat transfer rate. This is owing to the reason mentioned earlier in the introduction that the heat transfer is directly proportional to the thermal conductivity, density and the specific heat capacity and inversely proportional to the dynamic viscosity. Therefore, a critical examination for the microchannel heat sink is crucial as these thermophysical properties are different among the coolants, as seen in Figures 10 and 14.

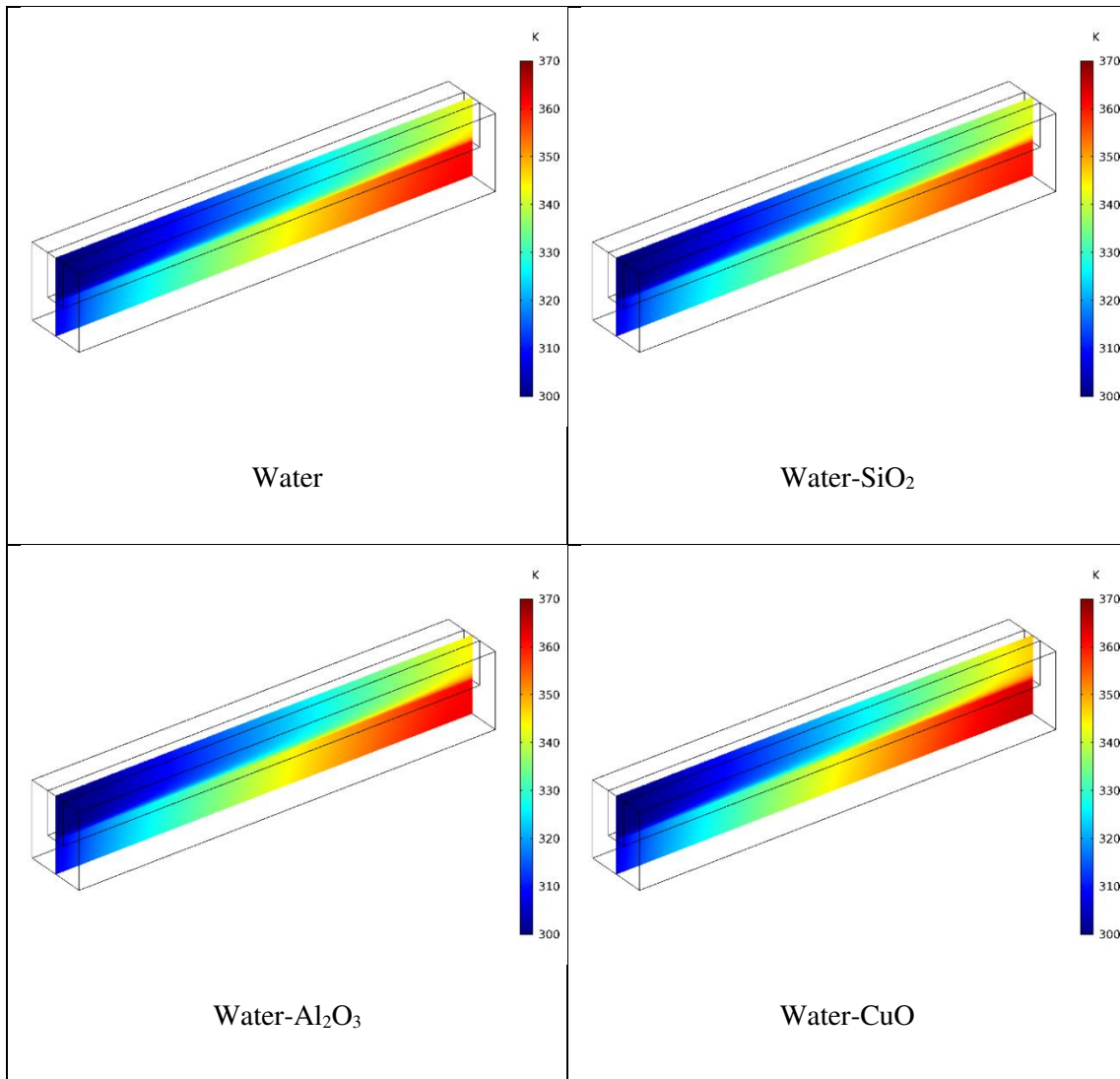
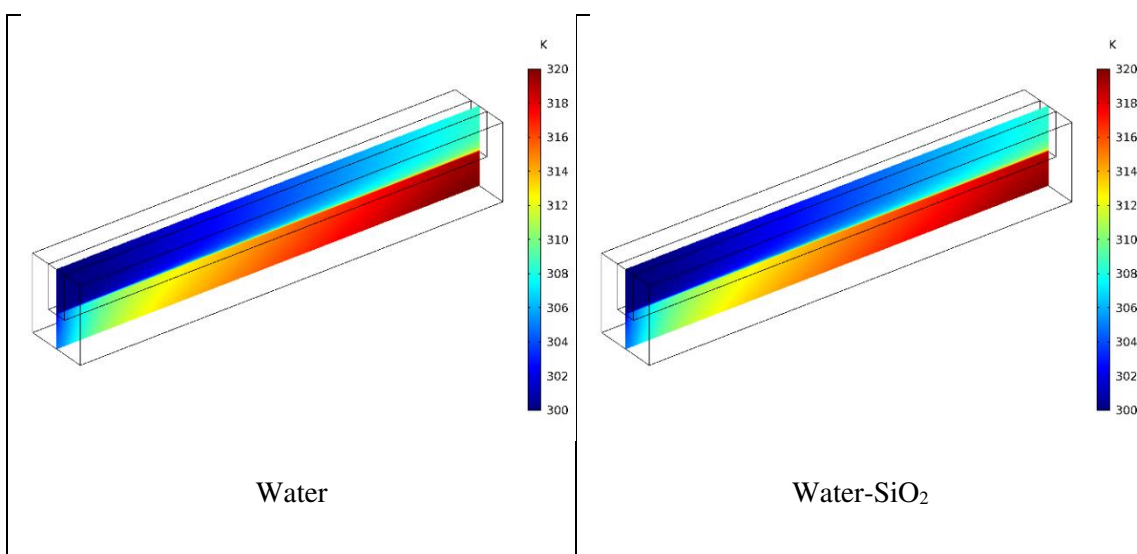


Figure 11. Temperature distributions in the microchannel heat sink at 100 Reynolds number.



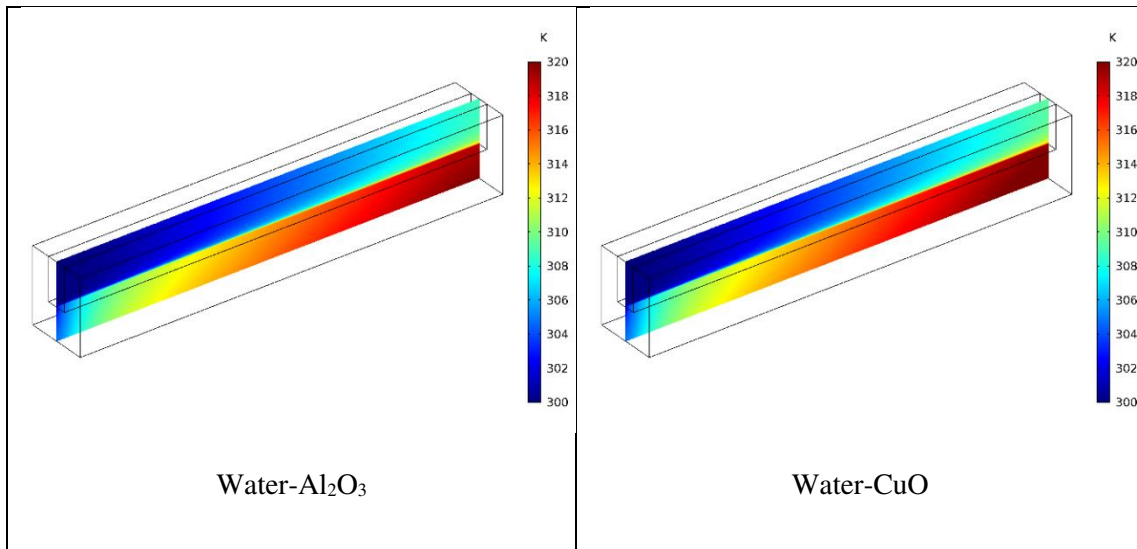


Figure 12. Temperature distributions in the microchannel heat sink at 500 Reynolds number.

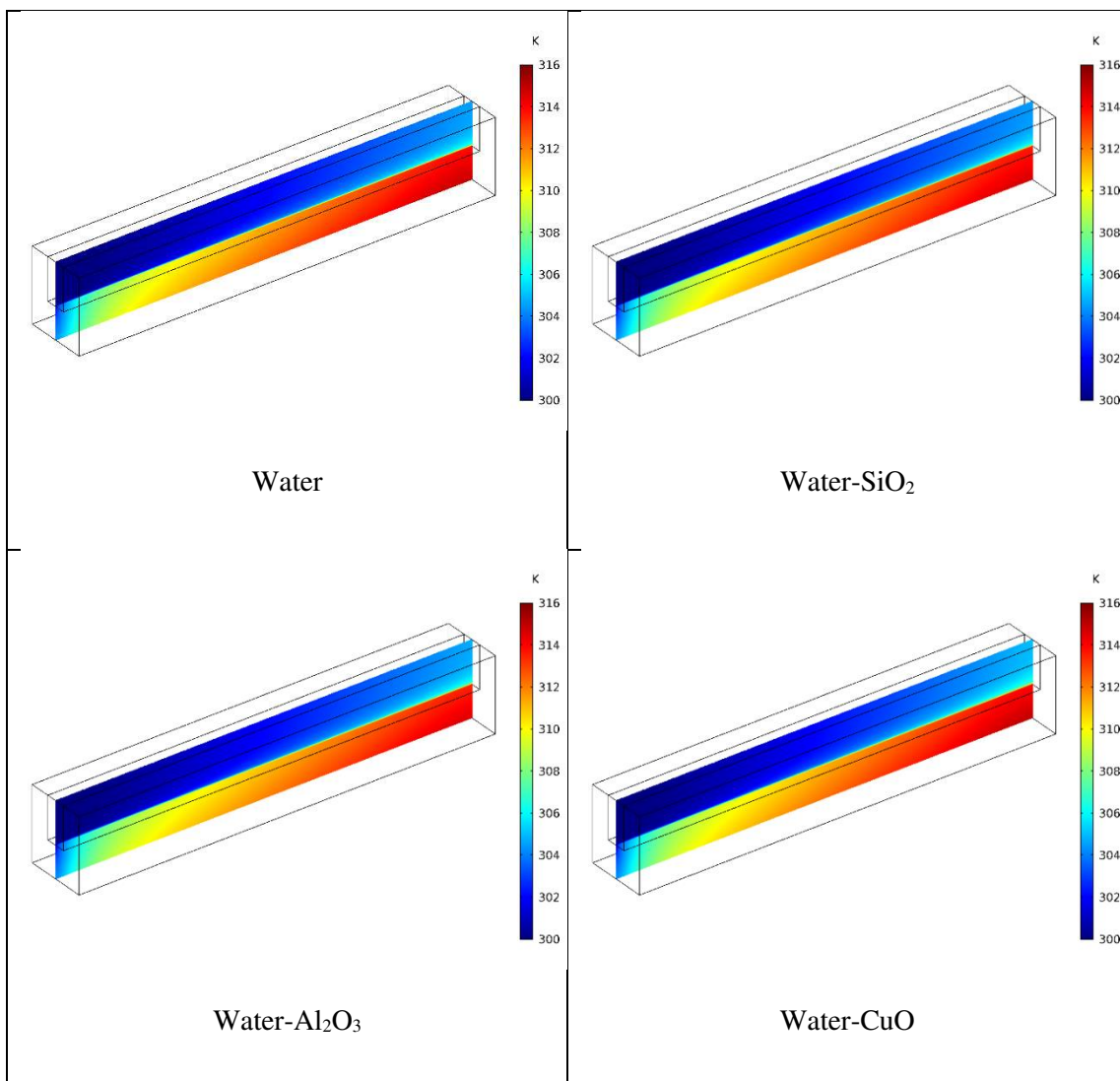


Figure 13. Temperature distributions in the microchannel heat sink at 900 Reynolds number.

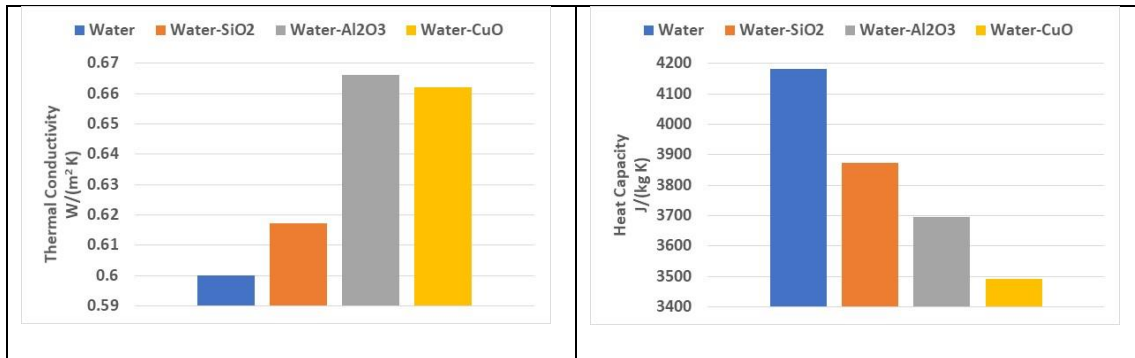


Figure 14. Thermal conductivity and heat capacity of different coolants.

### 3.4. Performance analysis

As mentioned in earlier, a critical examination of the microchannel heat sink is crucial, the heat transfer and fluid flow associated with several parameters for the microchannel heat sink has been presented and studied. The responses of the heat transfer coefficient, Nusselt number, thermal resistance, coolant pressure drop, and pumping power have been acquired for a range of Reynolds numbers to quantitatively represent the performance of the microchannel heat sink working through several types of coolants.

Figure 15 shows the heat transfer coefficient inside the microchannel heat sink. The figure shows that all kinds of nanofluids increase the coefficient of heat transfer. Comparison between nanofluids, the microchannel heat sink working with coolant of Al<sub>2</sub>O<sub>3</sub>-water has the highest value of the heat transfer coefficient for all the Reynolds numbers, due to it has the high thermal conductivity as compared with other nanofluids. However, the increase in the heat transfer coefficient is small especially at low Re (maximum enhancement is ~5% at Re = 900).

Figure 16 shows the Nusselt number of the microchannel heat sink. The Nu in the cases of water and water-SiO<sub>2</sub> are identical and higher than that of the water-Al<sub>2</sub>O<sub>3</sub> and water-CuO. However, the trend of changing of Nu with Re is the same for all the coolants (i.e., the rate change of Nu is higher at low Re than at high Re).

The maximum temperature of the microchannel's wall is shown in Figure 17 for the different coolants at different Re. at Re = 100, The maximum wall temperature in case of using water-CuO is the highest (~365 K). It is lower in case of water-Al<sub>2</sub>O<sub>3</sub> and lowest in case of water-SiO<sub>2</sub> and water. However, the differences in the maximum wall temperature converge as Re increases and they become identical when Re further increases (i.e., Re $\geq$ 500). The same trend can be seen in Figure 18, the average temperature of the coolants at the exit of the microchannel. The rate change of the temperatures in both figures is higher at low Re than that at high Re.

Figure 19 shows the thermal resistance of the microchannel heat sink. In literature, the thermal resistance is assumed to be an indication for the effectiveness of the microchannel heat sink. The thermal resistance depends on the inlet temperature of the coolant and the highest temperature at the wall of the microchannel heat sink. Obviously, RT decreases as Re increases for all coolants, and the curves become identical at high Re. Again, the rate change of RT is higher at low Re than that at high Re.

Figure 20 shows the pressure drop along the microchannel heat sink. The figure shows that the nanofluids have higher pressure drops than the base fluid (water), and they increase with the increase in the Reynolds numbers. Also, the pressure drop is clearly increasing in an exponential trend. This suggests that nanofluids might be beneficial at low Re as the heat transfer coefficient of nanofluids increases at higher rates at low Re as seen in Figure 15.

Practically, coolants that can reduce the wall temperature of the microchannel at lower pumping power is preferable. For this reason, the relationship between Re and pumping power is plotted in Figure 21. It is clear that water has the highest Re among other coolants at a certain pumping power. This is due to the low dynamic viscosity of water comparing to the other coolants. In general, the rate change of Re is higher at low pumping power than at higher pumping power. Therefore, it is necessary to examine the maximum wall temperature as functions of pumping power instead of Re.

Figure 22 shows the maximum wall temperature as function of the pumping power for the different coolants. It is obvious that the curves become coincided after the pumping threshold of 0.005 W. Also, water has the best performance at lower pumping power (i.e., less than 0.005 W). The maximum wall temperature decreases at very high rate for the low pumping power (less than 0.005 W) and at very low rate at power higher than 0.005 W. Consequently, employing water in microchannel heat sink at low pumping power is better than employing nanofluids. However, although the maximum wall temperature is the same for any coolant at high Re, using nanofluids is impractical due to the coherent issues such as aggregation and agglomeration, clogging and toxicity.

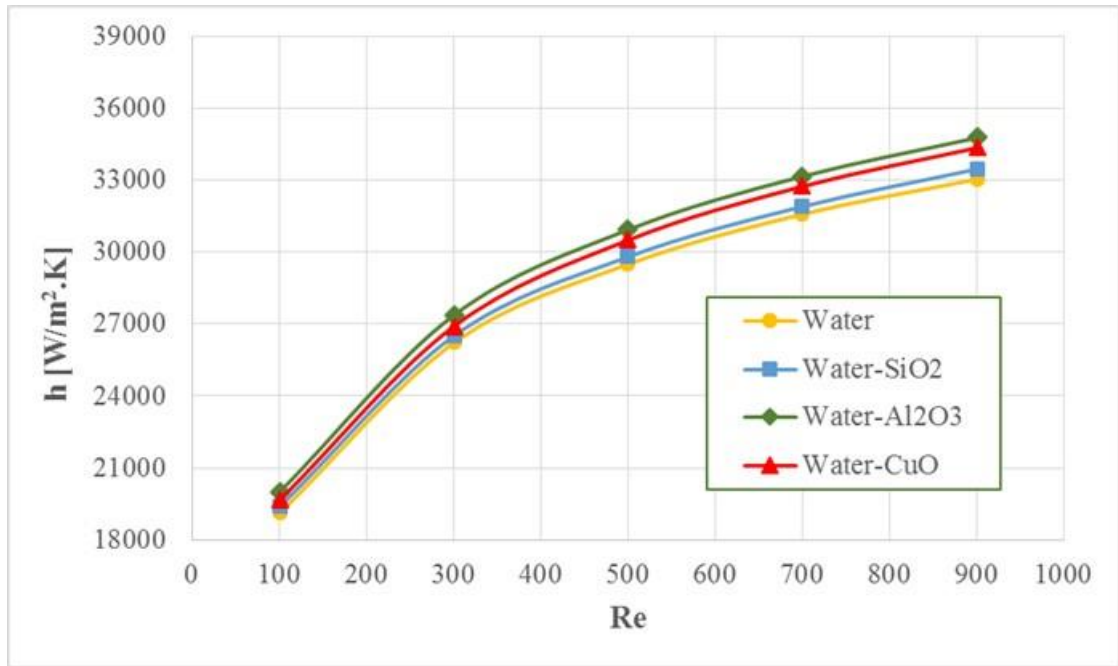


Figure 15. Variation of the heat transfer coefficient of the microchannel heat sink with Reynolds numbers for different coolants.

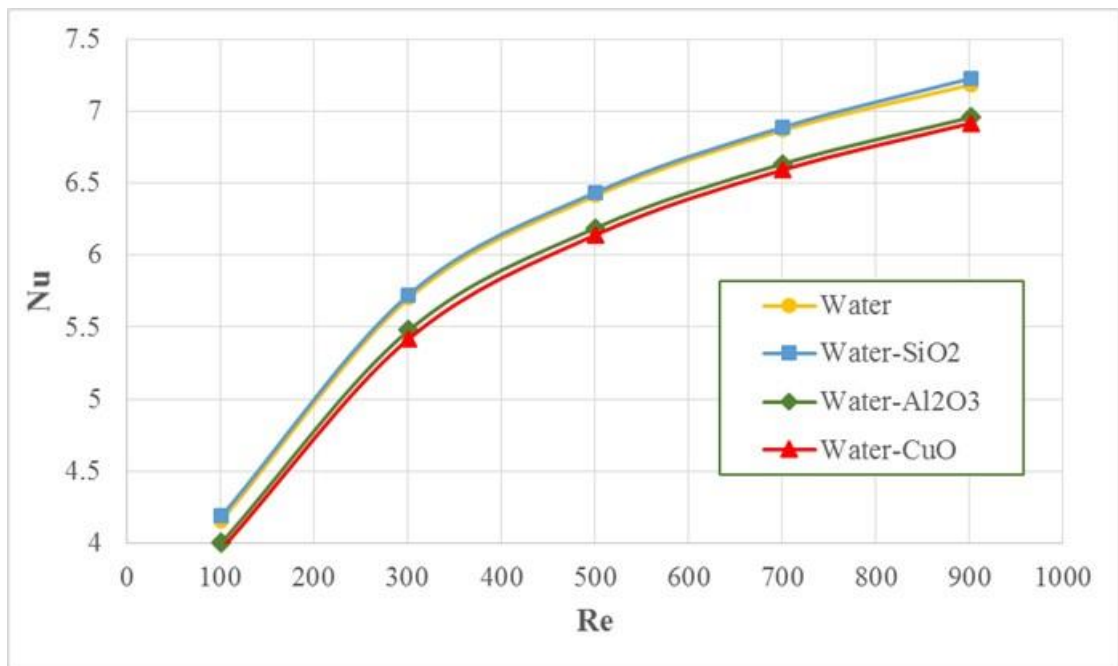


Figure 16. Variation of Nusselt number of microchannel heat sink with Reynolds numbers for different coolants.

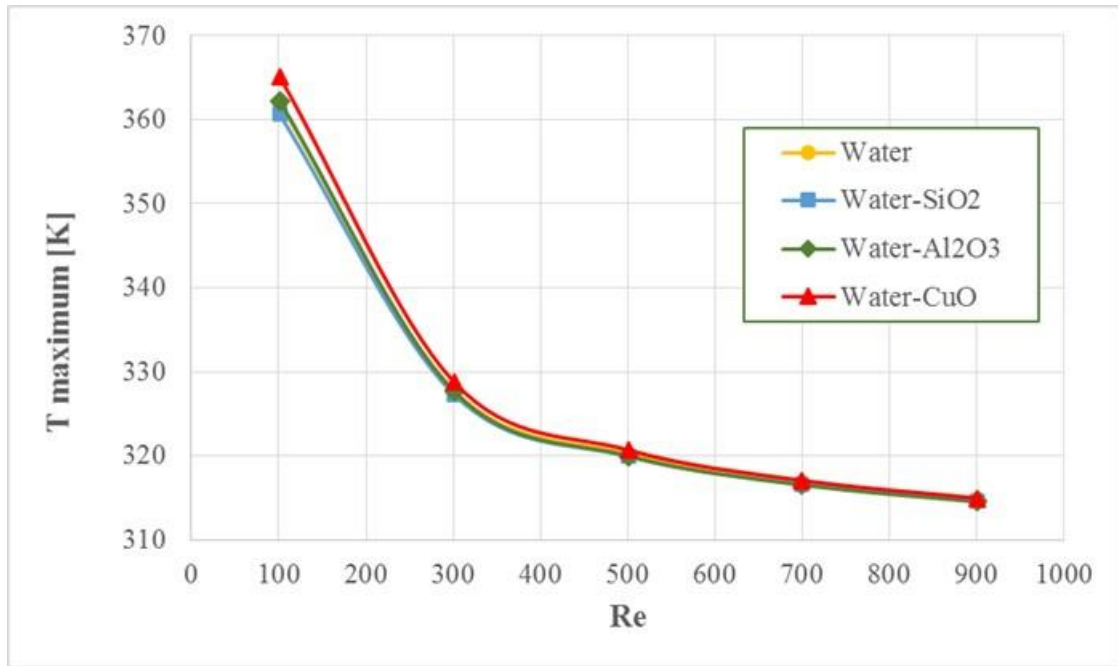


Figure 17. Maximum temperature of the channel's wall at a range of Re.

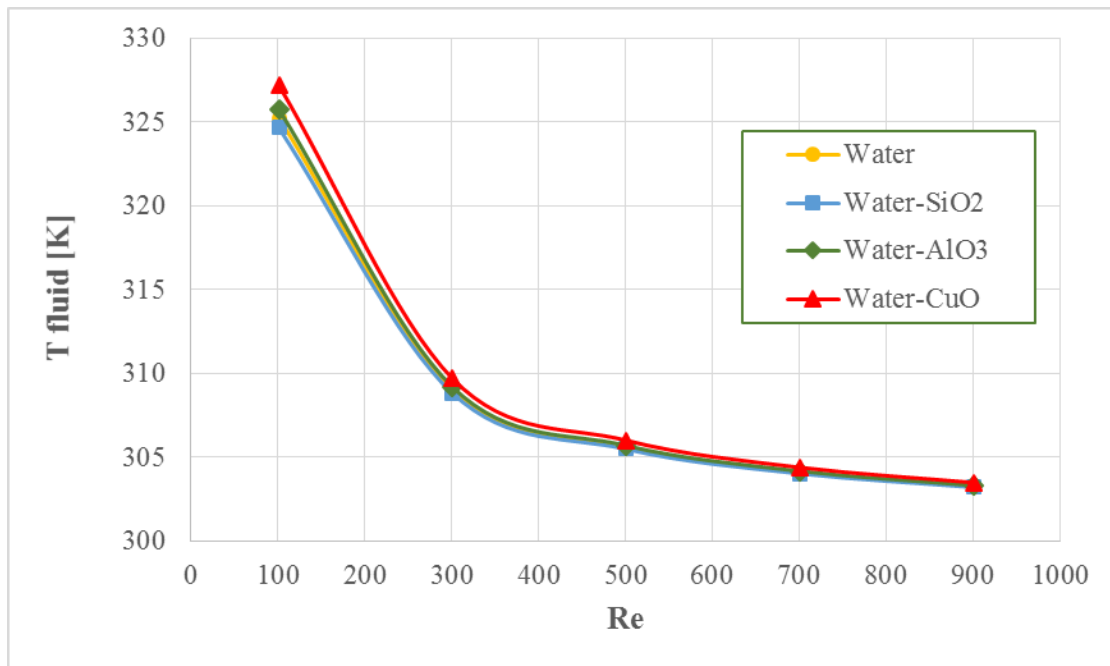


Figure 18. average temperature of the coolant at the exit of the channel at a range of Re.

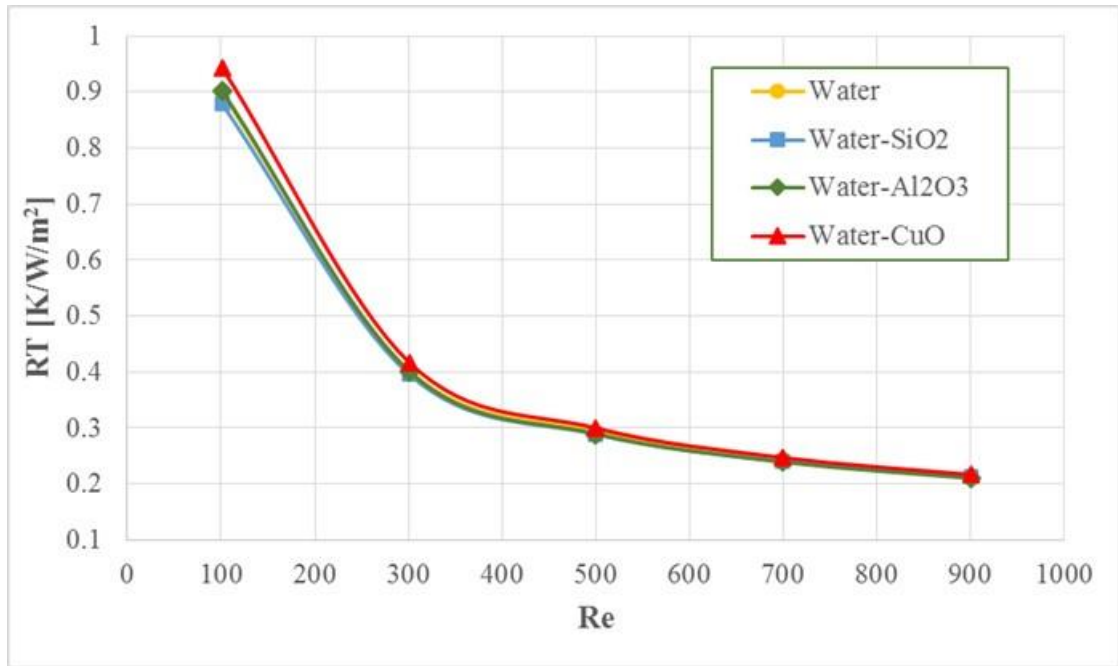


Figure 19. Variation of the thermal resistance of the microchannel heat sink with Reynolds numbers for several nanofluids.

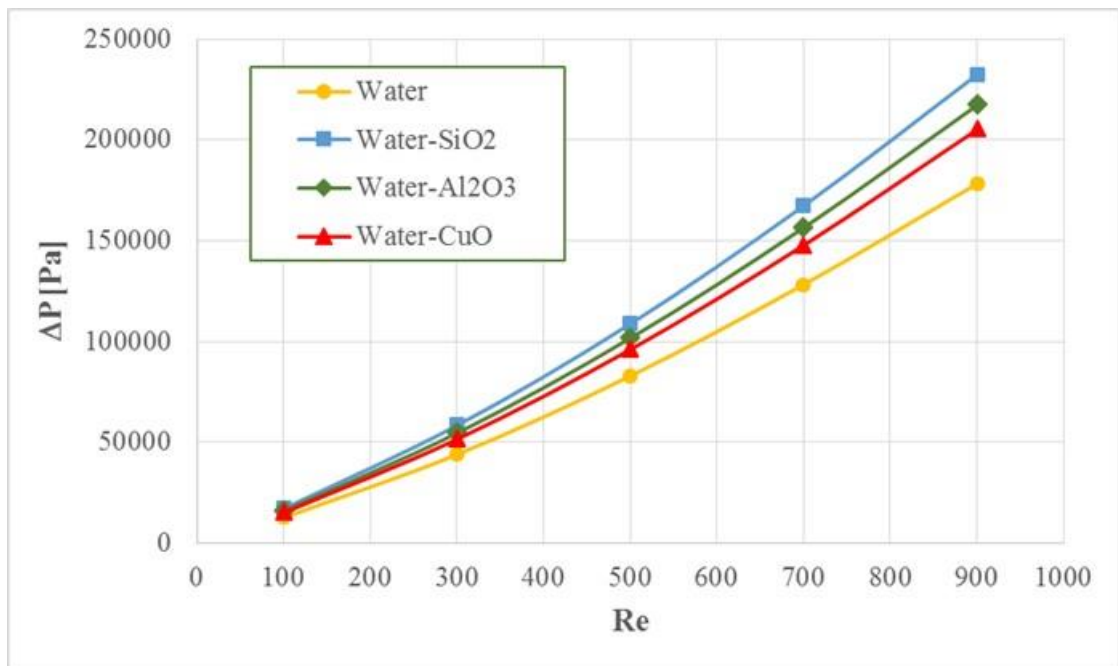


Figure 20. Variation of the pressure drop along the microchannel heat sink with Reynolds numbers for several nanofluids.

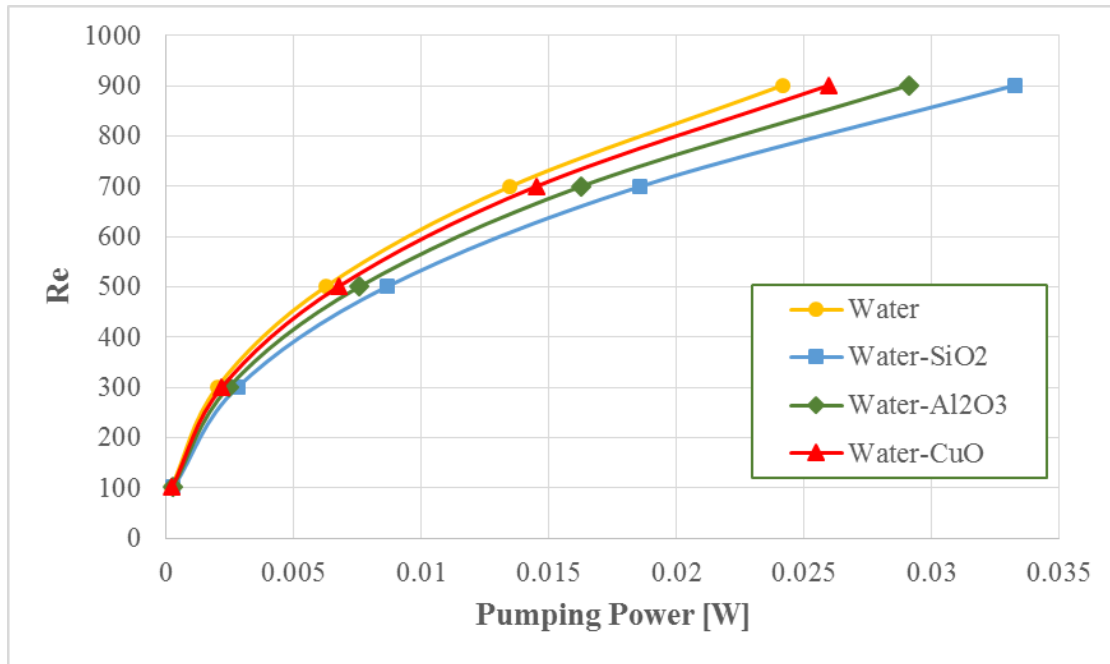


Figure 21. Variation of Re of different coolants with pumping power.

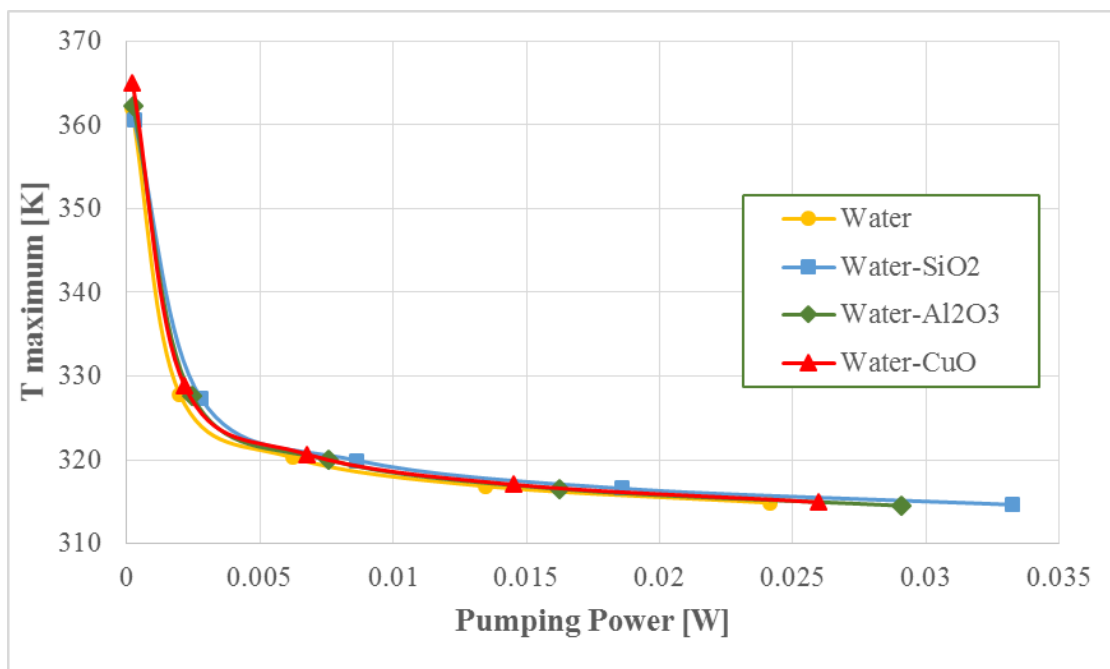


Figure 22. Maximum temperature of the channel's wall at a range of pumping power.

#### 4. Conclusion

This work develops a full three-dimensional, non-isothermal computational fluid dynamics (CFD) detailed model to study the thermal performance of the microchannel heat sink working with several coolants. The study revealed that studying the performance parameters of a microchannel heat sink as a function of Re is misleading due to the difference in the thermophysical properties of the different coolants. Nanofluids are impractical option to be employed in microchannel heat sinks and water is the practical one as it is cheaper and safer than the nanofluids.

#### References

- [1] H. A. Alhattab, M. A. R. Sadiq Al-Baghdadi, R. S. Hashim, and A. H. Ali, "Design of micro heat sink for power transistor by using CFD," *Al-Sadiq Int. Conf. Multidiscip. IT Commun. Tech. Sci. Appl. AIC-MITCSA 2016*, no. March 2018, pp. 268–272, 2016.
- [2] L. Chai, G. Xia, L. Wang, M. Zhou, and Z. Cui, "Heat transfer enhancement in microchannel heat sinks with periodic expansion – constriction cross-sections," *Int. J. Heat Mass Transf.*, vol. 62, pp. 741–751, 2013.
- [3] G. Xie, Z. Chen, B. Sunden, and W. Zhang, "Numerical Analysis of Flow and Thermal Performance of Liquid-Cooling Microchannel Heat Sinks with Bifurcation," *Numer. Heat Transf. , Part A Appl. An Int. J. Comput. Methodol.*, no. May 2014, pp. 37–41, 2013.
- [4] G. Xie, S. Li, B. Sunden, W. Zhang, and H. Li, "A numerical study of the thermal performance of microchannel heat sinks with multiple length bifurcation in laminar liquid flow," *Numer. Heat Transf. Part A Appl.*, vol. 65, no. 2, pp. 107–126, 2014.
- [5] L. Chai, G. Dong, and H. Sheng, "Parametric study on thermal and hydraulic characteristics of laminar flow in microchannel heat sink with fan-shaped ribs on sidewalls – Part 3 : Performance evaluation," *HEAT MASS Transf.*, 2016.
- [6] L. Chai, G. D. Xia, and H. S. Wang, "Parametric study on thermal and hydraulic characteristics of laminar flow in microchannel heat sink with fan-shaped ribs on sidewalls - Part 1: Pressure drop," *Int. J. Heat Mass Transf.*, vol. 97, pp. 1081–1090,

- 2016.
- [7] L. Chai, G. D. Xia, and H. S. Wang, "Parametric study on thermal and hydraulic characteristics of laminar flow in microchannel heat sink with fan-shaped ribs on sidewalls - Part 2: Pressure drop," *Int. J. Heat Mass Transf.*, vol. 97, pp. 1081–1090, 2016.
- [8] G. Lu, J. Zhao, L. Lin, X. Wang, and W. Yan, "A new scheme for reducing pressure drop and thermal resistance simultaneously in microchannel heat sinks with wavy porous fins," *Int. J. Heat Mass Transf.*, vol. 111, pp. 1071–1078, 2017.
- [9] R. Wang, J. Wang, B. Lijin, and Z. Zhu, "Parameterization Investigation on the Microchannel Heat Sink with Slant Rectangular Ribs by numerical simulation," *Appl. Therm. Eng.*, 2018.
- [10] H. Shen, C. Wang, and G. Xie, "A parametric study on thermal performance of microchannel heat sinks with internally vertical bifurcations in laminar liquid flow," *Int. J. Heat Mass Transf.*, vol. 117, pp. 487–497, 2018.
- [11] P. Li, Y. Luo, D. Zhang, and Y. Xie, "Flow and heat transfer characteristics and optimization study on the water-cooled microchannel heat sinks with dimple and pin-fin," *Int. J. Heat Mass Transf.*, vol. 119, pp. 152–162, 2018.
- [12] S. Lee, S. U. S. Choi, S. Li, and J. A. Eastman, "Measuring Thermal Conductivity of Fluids Containing Oxide Nanoparticles," *J. Heat Transfer*, vol. 121, no. 2, pp. 280–289, 1999.
- [13] S. U. S. Choi and J. A. Eastman, "ENHANCING THERMAL CONDUCTIVITY OF FLUIDS WITH NANOPARTICLES," *ASME International Mechanical Engineering Congress & Exposition*, 1995. [Online]. Available: <http://www.osti.gov/scitech/biblio/196525/>.
- [14] D. Wen, G. Lin, S. Vafaei, and K. Zhang, "Review of nanofluids for heat transfer applications," *Particuology*, vol. 7, no. 2, pp. 141–150, 2009.
- [15] J. Buongiorno *et al.*, "A benchmark study on the thermal conductivity of nanofluids," *J. Appl. Phys.*, vol. 106, no. 9, p. 094312, Nov. 2009.
- [16] D. C. Venerus *et al.*, "Viscosity measurements on colloidal dispersions (nanofluids) for heat transfer applications," *Appl. Rheol.*, vol. 20, no. 4, p. 2, 2010.

- [17] Maher A.R. Sadiq Al-Baghdadi, "A CFD analysis of transport phenomena and electrochemical reactions in a tubular-shaped ambient air-breathing PEM micro fuel cell," *Trans. Hong Kong Inst. Eng. (HKIE Trans.)*, vol. 17, no. 2, pp. 1–8, 2010.
- [18] Maher A.R. Sadiq Al-Baghdadi, "A CFD study of hygro-thermal stresses distribution in PEM fuel cell during regular cell operation," *Renew. Energy J.*, vol. 34, no. 3, pp. 674–682, 2009.
- [19] Maher A.R. Sadiq Al-Baghdadi, "Prediction of deformation and hygro-thermal stresses distribution in ambient air-breathing PEM fuel cells using three-dimensional CFD model," *Recent Patents Mech. Eng.*, vol. 2, no. 1, pp. 26–39, 2009.
- [20] S. Coskun, T. O.- Ozyurt, and H. E. Unalan, "Heat transfer enhancement by silver nanowire suspensions in microchannel heat sinks," *Int. J. Therm. Sci.*, vol. 123, 2018.
- [21] L. Snoussi, N. Ouerfelli, K. V. Sharma, N. Vrinceanu, A. J. Chamkha, and A. Guizani, "Numerical simulation of nanofluids for improved cooling efficiency in a 3D copper microchannel heat sink (MCHS)," *Phys. Chem. Liq.*, vol. 56, no. 3, pp. 311–331, 2018.
- [22] A. A. Alfaryjat, H. A. Mohammed, N. Mariah, D. Stanciu, and A. Dobrovicescu, "Numerical investigation of heat transfer enhancement using various nano fluids in hexagonal microchannel heat sink," vol. 5, no. September 2017, pp. 252–262, 2018.
- [23] M. T. Al-Asadi and W. T. Al-Sallami, "Do ionic liquids replace water or nanofluids to enhance heat transfer in micro-channel systems?," *MATEC Web Conf.*, vol. 240, pp. 13–15, 2018.
- [24] M. T. Al-asadi and M. C. T. Wilson, "Evaluation of nanofluids performance with vortex generators for enhanced micro-channel heat transfer," *ICTEA Int. Conf. Therm. Eng.*, no. February 2017, 2018.
- [25] M. Mital, "Evolutionary Optimization of Electronic Circuitry Cooling Using Nanofluid," vol. 2012, 2012.
- [26] H. R. Seyf and S. K. Mohammadian, "Thermal and Hydraulic Performance of Counterflow Microchannel Heat Exchangers With and Without Nanofluids," *J. Heat Transfer*, vol. 133, no. 8, p. 9, 2011.
- [27] F. S. Alkasmoul, M. T. Al-Asadi, T. G. Myers, H. M. Thompson, and M. C. T. Wilson, "A practical evaluation of the performance of Al<sub>2</sub>O<sub>3</sub>-water, TiO<sub>2</sub>-water and CuO-

- water nanofluids for convective cooling,” *Int. J. Heat Mass Transf.*, vol. 126, pp. 639–651, 2018.
- [28] B. Ghasemi and S. M. Aminossadati, “Brownian motion of nanoparticles in a triangular enclosure with natural convection,” *Int. J. Therm. Sci.*, vol. 49, no. 6, pp. 931–940, 2010.
- [29] L. Chai, G. Dong, and H. Sheng, “Numerical study of laminar flow and heat transfer in microchannel heat sink with offset ribs on sidewalls,” *Appl. Therm. Eng.*, vol. 92, pp. 32–41, 2016.